Edge-Dependent Topology in Kekulé Lattices

S. E. Freeney,[1,*] J. J. van den Broeke,[2,*] A. J. J. Harsveld van der Veen,[1] I. Swart,[1,†] and C. Morais Smith[2]
[1]Debye Institute for Nanomaterials Science, Utrecht University, Utrecht 3584 CC, Netherlands
[2]Institute for Theoretical Physics, Utrecht University, Utrecht 3584 CC, Netherlands

(Received 16 August 2019; accepted 11 May 2020; published 12 June 2020)

The boundary states of topological insulators are thought not to depend on the precise atomic structure of the boundary. A recent theoretical study showed that, for topological crystalline insulators with given bond strengths, topological states should only emerge for certain edge geometries. We experimentally probe this effect by creating artificial Kekulé lattices with different atomically well-defined edge geometries and hopping ratios in a scanning tunneling microscope. Topological edge modes are found to only appear for specific combinations of edge geometry and hopping ratio.

DOI: 10.1103/PhysRevLett.124.236404

A common assumption concerning topological states of matter is that their existence should be insensitive to any detail, except the topology of the bands. This is indeed the case for the quantum Hall [1–3] and quantum spin Hall [4–6] effects, which are triggered by a magnetic field and strong spin-orbit coupling, respectively. However, theory predicts that the edges of topological crystalline insulators are important [7,8]. The reason is that the topological invariant depends on the choice of unit cell, which also determines the edge geometry. To establish the relation between edge geometry and the existence of protected boundary states in topological crystalline insulators experimentally, it is essential to work with systems that have atomically precise edges.

Electrons in engineered potentials can be used to study the electronic properties of a large variety of systems [9–13]. Importantly, it is possible to control the hopping strength between different sites [9,14]. Vacancies in a chlorine monolayer on Cu(100) have been coupled together to realize topologically nontrivial domain-wall states in 1D Su-Schrieffer-Heeger chains [15]. In addition, the manipulation of Fe atoms on the superconducting Re(0001) surface led to a topological superconductor [16,17]. Recently, the carbon monoxide (CO) on Cu(111) platform was used to create robust corner localized zero energy modes in a 2D lattice [18]. This platform is therefore ideally suited to experimentally address the relation between the geometric structure of topological crystalline insulators and the emergence of nontrivial states.

We investigate this relation by focusing on the Kekulé lattice, see Fig. 1. The lattice consists of a triangular array of hexagonal molecules with intrahexagon bond strength t_0 (light blue lines), connected to each other by bonds of strength t_1 (navy lines). Gapless edge modes appear when the edge is connected only via weak bonds to the rest of the lattice. This topological crystalline system is protected by sublattice and mirror symmetry [19,20].

Here, we experimentally show that the same Kekulé structure may be trivial or topological, depending on the termination of the sample. The experimental observations are corroborated by theoretical calculations using muffin-tin and tight-binding approaches for the specific experimental realization, as well as investigations of the underlying crystalline symmetries protecting the topological phase.

To experimentally realize Kekulé lattices with atomically well-defined edges, we pattern the surface of a Cu(111) crystal with CO molecules, such that the surface state electrons form the desired structure [9]. All experiments were performed using a commercially available Scienta Omicron low-temperature scanning tunneling microscope (STM). Details of the procedures are given in the Supplemental Material [21] (see also [10,12,18]).

We generate finite lattices with two different hopping parameter ratios and two different edge terminations (bearded and molecular zigzag [19]). The geometry of the lattices is shown in Figs. 1(a) and 1(b). The leftmost column in Fig. 1 shows the precise positioning of the CO molecules on Cu(111) for a single Kekulé unit cell. Our designs are adjusted compared to those in Refs. [9,24] to minimize next-nearest neighbor hopping and to reduce building complexity. For $t_0 < t_1$, the repulsive potential introduced by the central six CO molecules diminishes the strength of t_0 (light blue). In contrast, for $t_1 < t_0$, there is less repulsion about the single central scatterer. Additionally, for $t_0 < t_1$, each triangularly shaped collection of four CO molecules reduces the bond strength between hexagons. For the $t_1 < t_0$ case, these tetramers are rotated by 60°. This allows for a stronger t_0, while simultaneously impinging on the connection between hexagons, decreasing t_1. We built triangular lattices to have the same edge geometry on all sides. Symmetry is locally preserved at the edges, including at the corners, where there is local resemblance to the edges. Interactions with the surrounding 2D electron gas were

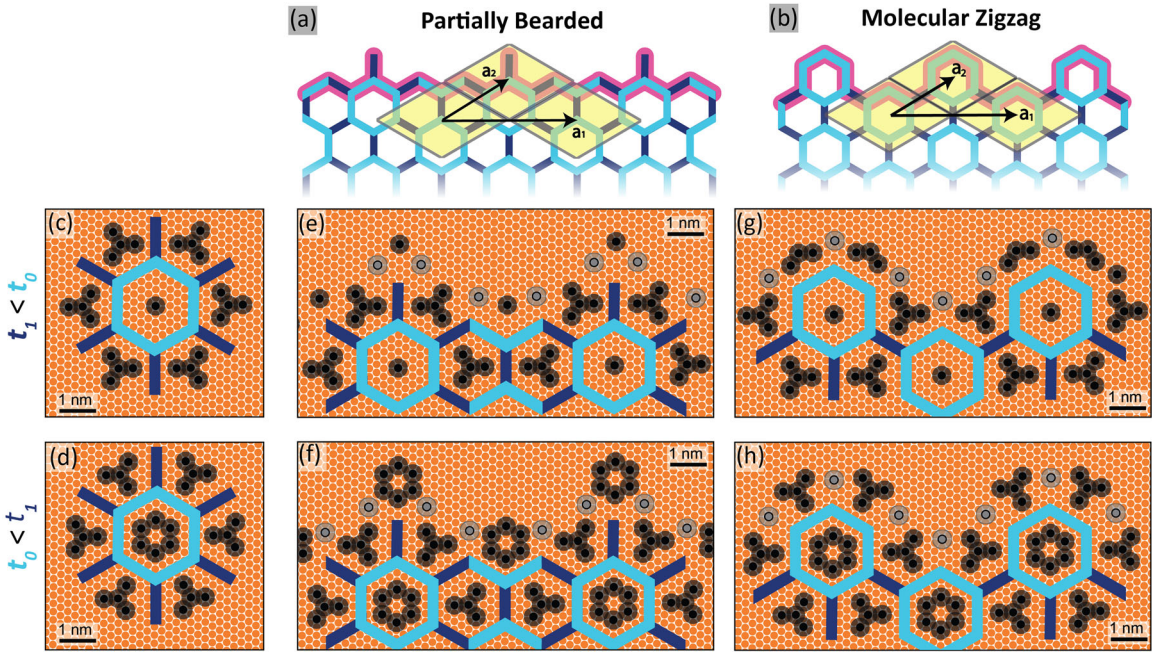

FIG. 1. (a),(b) Geometries of the partially bearded and molecular-zigzag edges. The light blue and navy lines indicate the intra- and interhexagon hopping parameters, respectively. The edges are highlighted in pink. The unit cell is defined by one yellow rhombus. $\boldsymbol{a_1}, \boldsymbol{a_2}$ indicate lattice vectors. The edge is formed by translation along $\boldsymbol{a_1}$. (c),(d) Configurations of CO molecules that lead to hopping regimes $t_1 < t_0$ and $t_0 < t_1$, respectively. (e)–(h) show the configurations of CO molecules to realize the partially bearded and molecular-zigzag edges in both hopping regimes. The gray circles represent additional CO molecules that reduce the interactions with the surrounding 2D electron gas.

minimized by adding additional CO molecules, see Supplemental Material [21].

To verify that the configuration of CO molecules leads to the appropriate hopping regime and to find the hopping parameters, the band structures calculated within the tight binding were matched to those calculated using the muffin-tin method [10,12,18]. In addition to the hopping parameters t_0 and t_1, orbital overlap and next-nearest neighbor (NNN) hopping were included in the tight-binding model. Detailed information is given in the Supplemental Material [21]. We find $t_1 = 0.7t_0$ and $t_0 = 0.67t_1$ for the configurations shown in Figs. 1(c) and 1(d), respectively. This confirms that the designs result in the desired parameter regime.

Although the orbital overlap deforms the band structure and is therefore of vital importance to understand the experimental results, it was numerically verified that it does not break the topological protection of the edge states in the Kekulé lattice. The NNN hopping, however, breaks chiral symmetry. It was found that most NNN hopping parameters were small ($\lesssim 0.02\ t_0$) due to the clustered CO structure. Only the NNN hopping within the hexagon for the $t_1 < t_0$ design ($0.2\ t_0$) is larger, as there is only one CO in the middle of the hexagons. Therefore, we expect that the chiral symmetry is weakly perturbed for that case.

Two different types of termination have been investigated for each lattice: the partially bearded edge and the molecular-zigzag edge [19]. Figure 1 shows both their geometric structure, as well as the configuration of CO molecules needed to realize these edges in both parameter regimes.

Two lattices with $t_1 < t_0$ are shown in Figs. 2(a) and 2(b). They have the same bulk but are terminated with a partially bearded and molecular-zigzag edge, respectively. Differential conductance spectra of bulk and edge sites of both lattices are shown in the middle panels of Figs. 2(a) and 2(b) [locations indicated by the colored dots in Figs. 2(a) and 2(b)]. The spectra of bulk and edge sites of the molecular-zigzag terminated lattice are similar, cf. black and blue curves in the middle panel of Fig. 2(b). In contrast, the local density of states (LDOS) of bulk and edges sites of the lattice with the partially bearded edge are markedly different. The spectrum of bulk sites (indicated in black) shows two peaks associated with the valence (at $V = -0.15$ V) and conduction bands ($V = 0.05$ V), separated by a gap. In contrast, the spectrum of the edge site (indicated in red) shows a large peak positioned at the energy of the bulk gap. The experimentally observed features are reproduced in the tight-binding [lower curves in the middle panels of Figs. 2(a) and 2(b)] and muffin-tin simulations, see Supplemental Material [21]. For the calculated LDOS, a broadening of 80 meV was added to account for the coupling between surface and bulk states [10,12,18,25].

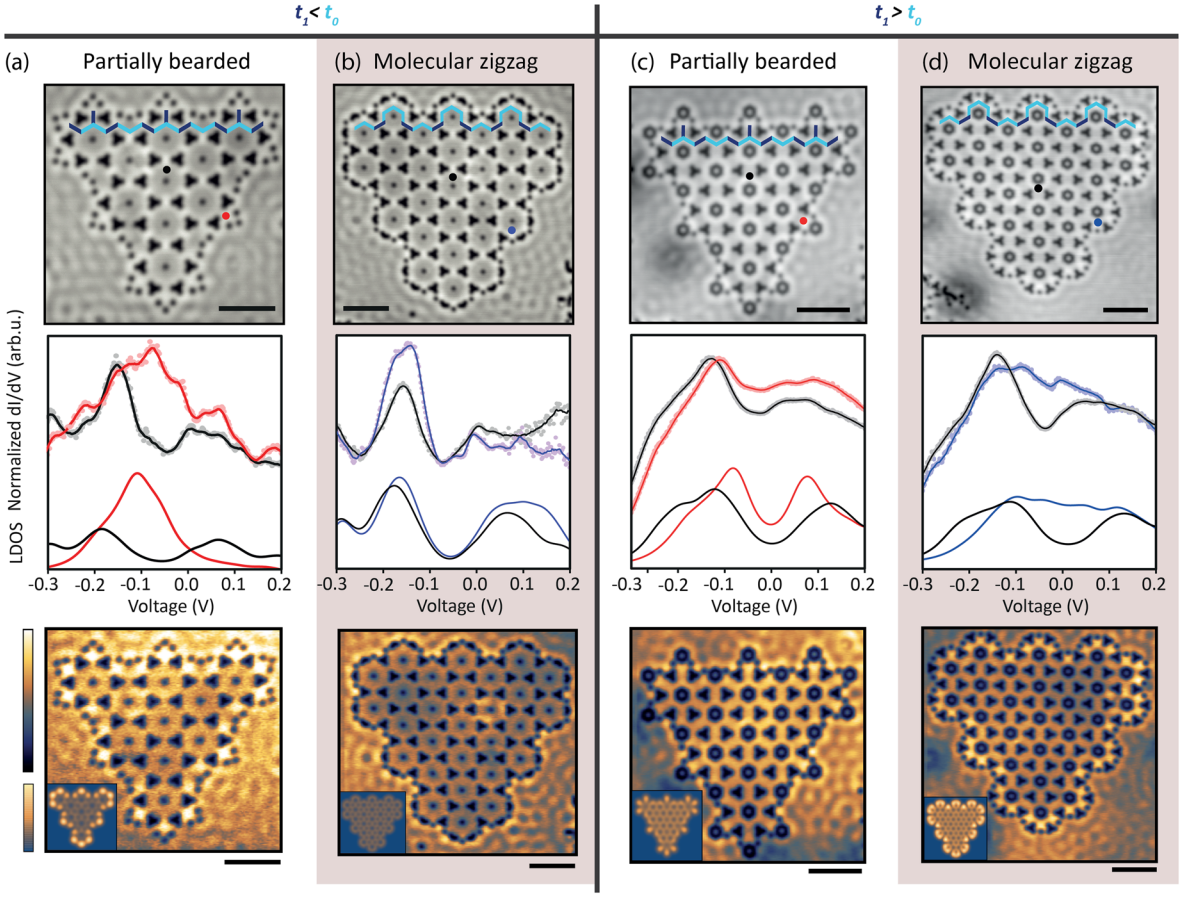

FIG. 2. (a) (Top) STM topograph of a Kekulé lattice with partially bearded edges and in the $t_1 < t_0$ regime ($V_{\mathrm{gap}} = 100$ mV, $I_{\mathrm{set}} = 10$ pA). Navy and light blue colors indicate bonds as depicted in Fig. 1. (a) (Middle) Experimental differential conductance spectra acquired at bulk (black) and edge (red) sites, normalized by spectra taken on Cu(111). Positions where spectra were acquired are indicated by colored dots in the top panel. The bottom curves depict the LDOS calculated using tight binding. (a) (Bottom) A differential conductance map acquired at a voltage close to the middle of the bulk gap ($V = -65$ mV). (Inset) The tight-binding LDOS map. (b) Same as (a), but now for a lattice with a molecular-zigzag edge. Settings for the topograph: $V_{\mathrm{gap}} = 100$ mV, $I_{\mathrm{set}} = 100$ pA. (c),(d) Same as (a),(b) but now for the opposite regime of hopping parameters, i.e., $t_1 > t_0$. Scan parameters for the topographs in (c),(d): $V_{\mathrm{gap}} = 100$ mV and $I_{\mathrm{set}} = 30$ pA. Differential conductance maps were acquired at -20 mV and the LDOS was calculated at -20 meV. Scale bars (black) are 5 nm.

The spatial extent of the in-gap state is probed by taking differential conductance maps at energies corresponding to the middle of the gap (approximately the on site energy of the system). By comparing the maps, shown in the bottom panels of Figs. 2(a) and 2(b), it is immediately clear that the bearded edge features a well-defined edge localized mode, whereas the lattice with molecular-zigzag edges in the same hopping regime does not. Again, the experimental features are reproduced in the simulations [see the insets in the bottom panels of Figs. 2(a) and 2(b)]. This edge localized state is robust with respect to the introduction of defects, see Supplemental Material [21].

These results support the theoretical prediction based on calculation of the topological invariant (the mirror winding number) [19] that the edge mode at the partially bearded edge is topological when $t_1 < t_0$.

The situation is reversed when the hopping strengths are inverted. Figures 2(c) and 2(d) show topographs and LDOS spectra for the Kekulé lattice in the opposite regime of hopping parameters, $t_0 < t_1$. In this case, for the partially bearded edge lattice [Fig. 2(c)], the experimental spectra at different edge positions match the behavior of the spectrum in the bulk of the crystal [Fig. 2(c), middle panel]: there is a dip in the experimentally measured LDOS around $V = -20$ mV for all positions, implying trivially insulating behavior throughout. At the molecular-zigzag edge [Fig. 2(d)] for the same $t_0 < t_1$ case, there is a markedly higher LDOS at the edge positions at energies corresponding to the bulk gap [Fig. 2(d), middle panel]. The differential conductance maps confirm that, for this parameter regime, the molecular-zigzag terminated lattice features a topological edge mode. The theoretical spectra and maps agree with the experimental data [see inset in Fig. 2(d)].

From these results, we conclude that nontrivial edge modes in topological crystalline insulators in a given regime of hopping parameters only emerge for specific edge geometries. The topological protection occurs at the Γ point and remains robust as long as the bulk states do not mix with the edge states in the middle of the bulk gap. Our experimental broadening is small enough that we do not expect it to influence the topological protection.

Finally, we turn our attention to finite-size effects. We first study how edge states are protected in the ribbon geometry and then investigate how these features change for the finite structures built experimentally. Kariyado and Hu [19] found that the mirror winding number protects the zero energy crossing of the edge modes in the Kekulé system. The calculation of this invariant requires both reflection symmetry M_y (the mirror plane intersects the middle of the unit cell and is perpendicular to the edge) and chiral symmetry. Therefore, both symmetries need to be present to protect the edge states. This has been confirmed by Noh *et al.* [20] by numerically adding perturbations to the Hamiltonian. In the case of armchair terminated Kekulé lattices, the M_y symmetry is broken and the edge modes become gapped.

When a system can be divided in two subsystems that only couple to each other and never to themselves, the system possesses chiral symmetry. The chiral symmetry leads to a spectrum that is symmetric around zero energy. This means that zero modes can only move away from zero energy in pairs. If there are more sites of one subsystem than of the other on the edge, but not in the rest of the structure, this can result in zero modes on the edge, as in graphene ribbons with a zigzag termination [26,27]. The edge geometry considered here contains equally many sites of each sublattice. Thus, chiral symmetry alone does not enforce the existence of edge states. To understand the protection of zero modes in the system, we should therefore also consider the reflection symmetry M_y. At the Γ point in the Brillouin zone, M_y commutes with the Hamiltonian. Hence, the Hamiltonian needs to have the same eigenstates as M_y, and states that are even and odd under M_y cannot mix. This mechanism prevents two zero modes on the edge of a Kekulé ribbon to mix, thus pinning them at zero energy due to the chiral symmetry.

The Kekulé lattices realized here have (approximate) chiral symmetry, since the NNN hopping is small. The M_y symmetry is preserved locally. In the experimental designs, the lattice sites are locally affected by the same environment as they would be in an infinitely long ribbon, as illustrated in Fig. 3(a). However, the global mirror symmetry present in the ribbon is broken in the finite lattice: the boundary is not fully periodic due to modulations to form the corner. Moreover, the lattice is relatively small; thus, the momenta are not continuous and a state with zero momentum (the Γ point) does not need to exist. By performing tight-binding calculations on finite molecular-zigzag terminated lattices, we determine the evolution of the energy levels upon tuning the ratio t_0/t_1. Figure 3(b) shows this for a lattice with the same size as the experimental system. The in-gap energy levels obtained for a fixed ratio of t_0/t_1 are continuous lines for infinite systems, but become discrete dotted lines (coarse grained) for finite-sized systems. The smaller the system, the larger the distance between the dots. Nevertheless, the spreading and the number of edge states do not change with the size of the system [21]. Because of hybridization of the edge modes in this finite-size system, the edge modes move away from zero energy before the phase transition at $t_0 = t_1$. For larger systems, the edge modes remain close to zero energy for a longer parameter range, as shown in the Supplemental Material [21]. Note that, since the edge states here are dispersive, they span the entire bulk band gap.

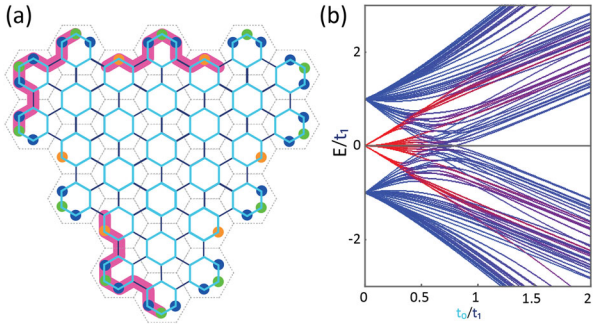

FIG. 3. (a) Illustration of the finite molecular-zigzag terminated lattice. Green represents protruding sites that couple weakly to two blue sites; orange represents sites sitting in a "cove" at the edge of the lattice. The sections shown in pink have the same local environment. (b) Energy spectrum as a function of t_0/t_1. The spectrum is shown for the system size used in the experiments with 28 hexagons in total. The coloring of the points signifies the localization of the states. Fully edge localized states appear red; bulk localized states appear blue. The color value was determined for each point by summing over the tight-binding wave function edge (bulk) components squared to get the red (blue) contribution.

In conclusion, by studying Kekulé lattices with two different bulk structures and two types of edge termination, we investigated the influence of the boundary shape on the existence of nontrivial edge modes in topological crystalline insulators. We found that, for the same bulk, the existence of nontrivial edge modes depends on the termination of the sample.

The detection of 1D edge modes in this finite-size 2D system is remarkable. In translational invariant ribbons, the mirror and chiral symmetries pin the edge modes to zero energy at the Γ point in the Brillouin zone. However, here we investigate a finite and relatively small system, without translational symmetry and for which a Brillouin zone cannot be defined. Furthermore, in the $t_1 < t_0$ regime, chiral symmetry is not strictly enforced due to a nonzero NNN hopping, and the mirror symmetry is not globally

preserved. This suggests that the edge modes are remarkably robust to weak symmetry breaking and finite-size effects. Finally, this Letter highlights the potential of using artificial lattices to study topological states of matter.

We acknowledge Marcel Franz for fruitful discussions. I. S. and C. M. S. acknowledge funding from NWO via Grants No. 16PR3245 and No. DDC13.

*These authors contributed equally.
†I.Swart@uu.nl

[1] K. Von Klitzing, Rev. Mod. Phys. **58**, 519 (1986).
[2] D. J. Thouless, M. Kohmoto, M. P. Nightingale, and M. den Nijs, Phys. Rev. Lett. **49**, 405 (1982).
[3] A. Altland and M. R. Zirnbauer, Phys. Rev. B **55**, 1142 (1997).
[4] C. L. Kane and E. J. Mele, Phys. Rev. Lett. **95**, 226801 (2005).
[5] B. A. Bernevig, T. L. Hughes, and S.-C. Zhang, Science **314**, 1757 (2006).
[6] M. König, S. Wiedmann, C. Brüne, A. Roth, H. Buhmann, L. W. Molenkamp, X.-L. Qi, and S.-C. Zhang, Science **318**, 766 (2007).
[7] L. Fu, Phys. Rev. Lett. **106**, 106802 (2011).
[8] R.-J. Slager, A. Mesaros, V. Juričić, and J. Zaanen, Nat. Phys. **9**, 98 (2013).
[9] K. K. Gomes, W. Mar, W. Ko, F. Guinea, and H. C. Manoharan, Nature (London) **483**, 306 (2012).
[10] M. R. Slot, T. S. Gardenier, P. H. Jacobse, G. C. van Miert, S. N. Kempkes, S. J. Zevenhuizen, C. M. Smith, D. Vanmaekelbergh, and I. Swart, Nat. Phys. **13**, 672 (2017).
[11] L. C. Collins, T. G. Witte, R. Silverman, D. B. Green, and K. K. Gomes, Nat. Commun. **8**, 15961 (2017).
[12] S. Kempkes, M. Slot, S. Freeney, S. Zevenhuizen, D. Vanmaekelbergh, I. Swart, and C. M. Smith, Nat. Phys. **15**, 127 (2019).
[13] M. Nurul Huda, S. Kezilebieke, and P. Liljeroth, arXiv: 2003.08234.
[14] J. Girovsky, J. L. Lado, F. E. Kalff, E. Fahrenfort, L. J. J. M. Peters, J. Fernández-Rossier, and A. F. Otte, Sci. Post. Phys. **2**, 020 (2017).
[15] R. Drost, T. Ojanen, A. Harju, and P. Liljeroth, Nat. Phys. **13**, 668 (2017).
[16] H. Kim, A. Palacio-Morales, T. Posske, L. Rózsa, K. Palotás, L. Szunyogh, M. Thorwart, and R. Wiesendanger, Sci. Adv. **4**, eaar5251 (2018).
[17] A. Kamlapure, L. Cornils, J. Wiebe, and R. Wiesendanger, Nat. Commun. **9**, 3253 (2018).
[18] S. Kempkes, M. Slot, J. van den Broeke, P. Capiod, W. Benalcazar, D. Vanmaekelbergh, D. Bercioux, I. Swart, and C. M. Smith, Nat. Mater. **18**, 1292 (2019).
[19] T. Kariyado and X. Hu, Sci. Rep. **7**, 16515 (2017).
[20] J. Noh, W. A. Benalcazar, S. Huang, M. J. Collins, K. P. Chen, T. L. Hughes, and M. C. Rechtsman, Nat. Photonics **12**, 408 (2018).
[21] See Supplemental Material at http://link.aps.org/supplemental/10.1103/PhysRevLett.124.236404 for details of the experimental and theoretical methods, a discussion on the influence of the surrounding 2DEG and defects, and theoretical results on larger lattices, which includes Refs. [22,23].
[22] D. Nečas and P. Klapetek, Open Phys. **10**, 181 (2012).
[23] S. Li, W.-X. Qiu, and J.-H. Gao, Nanoscale **8**, 12747 (2016).
[24] L.-H. Wu and X. Hu, Sci. Rep. **6**, 24347 (2016).
[25] M. R. Slot, S. N. Kempkes, E. J. Knol, W. M. J. van Weerdenburg, J. J. van den Broeke, D. Wegner, D. Vanmaekelbergh, A. A. Khajetoorians, C. Morais Smith, and I. Swart, Phys. Rev. X **9**, 011009 (2019).
[26] K. Nakada, M. Fujita, G. Dresselhaus, and M. S. Dresselhaus, Phys. Rev. B **54**, 17954 (1996).
[27] M. Fujita, K. Wakabayashi, K. Nakada, and K. Kusakabe, J. Phys. Soc. Jpn. **65**, 1920 (1996).